

Hyperbolic wavelet-Fisz denoising for a model arising in ultrasound imaging

Younes Farouj, Jean-Marc Freyermuth, Laurent Navarro, Marianne Clausel, and Philippe Delachartre

Abstract—We present an algorithm and its fully data-driven extension for noise reduction in ultrasound imaging. The proposed method computes the hyperbolic wavelet transform of the image, before applying a multiscale variance stabilization technique, via a Fisz transformation. This adapts the wavelet coefficients statistics to the wavelet thresholding paradigm. The use of hyperbolic wavelets makes it possible to recover the image while respecting the anisotropic nature of structural details. The data-driven extension obviates the need for any prior knowledge of the noise model parameters by estimating the noise variance using an isotonic Nadaraya-Watson estimator. Experiments on synthetic and real data demonstrate the potential of the proposed algorithm to recover ultrasound images while preserving tissue details. Furthermore, comparisons with other noise-reduction methods show that our technique is competitive with the state-of-the-art OBNLM filter. Finally, the variance estimation procedure is applied to real images emphasizing the noise model.

Index terms— Hyperbolic wavelets, Fisz transformation, Variance stabilization, Gaussianization, Ultrasound imaging, Data-driven denoising.

I. INTRODUCTION

ULTRASOUND (US) imaging has been a well-established diagnostic tool in various medical applications for many years. This technology remains one of the least expensive and safest among medical imaging modalities. Nevertheless, the examination and interpretation of ultrasound images is particularly challenging. This is mainly due to the presence of a particular type of noise called “speckle”, which can also be found in similar imaging systems such as synthetic aperture radar (SAR) and laser imaging. In ultrasound imaging, acquired signals are adjusted inside the scanner, prior to

This work was supported by “Région Rhône-Alpes” under the ARC 6. M. Clausel’s research is supported by the French Agence Nationale de la Recherche (ANR) under reference ANR-13-BS03-0002-01 (ASTRES) and PERSYVAL-Lab (ANR-11-LABX-0025-01). L. Navarro’s research is supported by the (ANR) under reference ANR-15-CE19-0002 (LBSMI). P. Delachartre is within the framework of the Labex CELYA (ANR-10-LABX-0060) of the Université de Lyon. J.-M. Freyermuth’s research was supported by the Engineering and Physical Sciences Research Council [EP/K021672/2]

Y. Farouj and P. Delachartre are with the Université de Lyon; CREATIS; CNRS UMR5220; Inserm U1044; INSA-Lyon; Lyon 69622, France (e-mail: farouj@creatis.insa-lyon.fr; delachartre@creatis.insa-lyon.fr).

J.-M. Freyermuth is with the Statistical Laboratory, DPMMS, University of Cambridge, Cambridge, CB3 0WB (e-mail: jean-marc.freyermuth@kuleuven.be).

L. Navarro is with the Ecole Nationale Supérieure des Mines; CIS-EMSE; CNRS UMR 5307; LGF, F-42023 Saint-Etienne, France (e-mail: navarro@emse.fr).

M. Clausel is with the Université de Grenoble; Laboratoire Jean Kuntzmann; CNRS UMR 5224, Grenoble, France (e-mail: marianne.clausel@imag.fr).

display, by a nonlinear processing transformation called *log-compression* [1]. This process aims at enhancing backscatterers in order to facilitate visual understanding. In this paper, we develop a novel methodology to recover ultrasonic images using a relevant signal-dependent noise model [2] that takes into account the modification of noise characteristics due to the *log-compression*. Adaptations of non-local and variational techniques to this model have already been described in the literature by Coupé *et al.* [3] and then Jin and Yang [4].

Although these methods lead to convincing results in terms of the signal-to-noise ratio, they still produce displeasing visual quality, mostly characterized by attenuated sharp edges. In this paper we present a different strategy that belongs to the wavelet denoising approaches [5]. As in the majority of denoising approaches, the wavelet denoising paradigm is based on the constraining assumption that the noise is additive white Gaussian noise (AWGN). To go beyond this case, we adapt a multiscale variance stabilization technique introduced by Fryzlewicz [6] in order to make the distribution of wavelet coefficients asymptotically Gaussian with the same variance. We extend this method to hyperbolic wavelets and show how variance stabilization can be easily performed using the low-frequency outputs from the wavelet transform at different scales. The motivation behind the use of hyperbolic wavelets is their capacity to provide better estimators than the standard wavelet-tensor construction when images contain anisotropic features [7][8][9]. Anisotropy has been promoted in many studies related to ultrasound image denoising (e.g. see [10], [11] and [12]) as often occurs due to the presence of features such as skin layers and vessels. Our algorithm consists of the following steps: (1) compute the wavelet transform of the image; (2) estimate local means using the approximation coefficients of the wavelet transform at each scale; (3) evaluate the variance function for each local mean component; (4) compute the Fisz-transformation of the wavelet coefficients: each coefficient is divided by the estimated local variance to stabilize the coefficients; (5) hard thresholding: keep the coefficients obtained in step (1) whose Fisz-transformed versions have magnitudes larger than a given threshold.

Finally, we show how our approach can be performed in a blind mode, that is, without any prior knowledge of the noise variance. This involves the use of a mean filter for a pre-estimation of the image. The variance function is then estimated using a Nadaraya-Watson estimator.

To validate these methods, we present numerical experiments based on synthetic and real data, and a comparative study with the state-of-the-art non-local and variational algorithms. We demonstrate that our data-driven approach

performs nearly as well as in situations where the noise variance is known. Moreover, the variance measured on real ultrasound images confirms the relevance of the noise model being considered.

The rest of the paper is organized as follows. A brief overview of different US noise models and dedicated denoising techniques is presented in section II. In section III, we describe our novel wavelet-based methodology. Finally, extensive experimental results and comparisons are provided in section IV.

II. IMAGE FORMATION AND RELATED WORK

Medical US imaging consists in transmitting a collection of ultrasonic waves, from a probe (an array of transducers), into the body. While propagating, these waves interact with different tissues and are reflected back by the scatterers to the transducers. The echoes are converted back into electrical impulses giving the so-called radio-frequency (RF) signals. These signals are then analyzed to retrieve the depth and the strength of the echoes, thus forming the US image from the amplitudes and the locations of the scatterers. Before display, the RF signals are post-processed. The high-frequency carrier is suppressed via a demodulation step (envelope detection). The dynamic range of the obtained signals is, however, too large for human visual perception. To overcome this, a process called logarithmic compression [1] is used to enhance the backscatterers.

US speckle noise results from the coherent accumulation of individual scattered beams from tissue inhomogeneities. It can be shown that the sum of the contributions of these scatterers within a resolution cell is normally distributed [13]. Novel techniques emerging in the general image processing community have been continuously adapted to remove US speckle noise. Hereafter, an overview of the main models and techniques is proposed.

A. Multiplicative Noise

An important challenge in developing novel methods for denoising ultrasound images is to find an adequate noise model. One can derive a natural noise model from the statistics of the echo signals. It can be shown that after the demodulation step, the distribution of the magnitude image is no longer Gaussian but rather Rayleigh [14]. This understanding gave rise to multiplicative noise models similar to those used in SAR imaging. Many filters have been proposed for such models, including the seminal works by Lee [15], Frost *et al.* [16] and Kuan [17]. Anisotropic diffusion filters [18] have also been successful in US imaging. These include adaptations to account for speckle noise statistics as in the speckle-reducing-anisotropic-diffusion (SRAD) [10], its oriented version (OSRAD) [11], and more recently, memory-driven filters [12].

B. Additive Noise

Multiplicative noise models do not take into consideration the logarithmic compression leading to the final US images visualized on the scanners. A simple solution is to assume that the signal and the noise are totally distinct. Thus, the

logarithmic compression step transforms the multiplicative noise model into an additive signal-independent noise model:

$$v = u + \varepsilon, \quad (1)$$

where v is the observation, u is the unknown image and ε is a random noise component. Wavelet-based methods have been considered to deal with this type of model depending on the nature of ε . For example, Zong *et al.* [19] assumed that ε is a zero-mean Gaussian white noise, which leads to AWGN models that are perfectly suited for the classical wavelet thresholding approaches [5]. Achim *et al.* [20] showed that under model (1) and logarithmic transformations, the wavelet coefficients of the noise component ε have non-Gaussian statistics that can be described by some alpha-stable distributions [21] and customized the wavelet thresholding for such a situation.

C. Hybrid Noise

The main drawback of model (1) is that it does not take into account the assumption that the noise level is proportional to the underlying image intensity. This assumption is widely used and accepted in echography. For example, it is the key idea behind motion estimation via speckle tracking [22]. The logarithmic compression can make the statistics of ultrasound images deviate from the Rayleigh distribution [23]. For instance, a Fisher-Tippett distribution was used in [24] to distinguish between tissues in segmentation tasks. A relevant model for ultrasound noise removal was presented in [2] and assumes that the variance of the noise component is no longer constant but respects the following equation:

$$v = u + u^\gamma \varepsilon, \quad (2)$$

where ε is a zero-mean Gaussian white noise $\varepsilon \sim \mathcal{N}(0, \sigma^2)$, with $\sigma \in (0, \infty)$, and $\gamma > 0$. Model (2) seems to be more appropriate as it preserves the signal dependency and has shown been to be effective for speckle modeling [2], as well as motion estimation in US image sequences [25]. This model has the advantage of being general and flexible. In fact, the parameter γ can be adapted to catch the image statistics depending on the post-processing inside the scanner. In this paper, we develop an appropriate wavelet thresholding method assuming that model (2) holds true. Adaptations of two other classical paradigms in denoising, in addition to wavelet methods, have been studied for model (2) [3][4]. We recall these paradigms:

Non-local methods. The non-local point of view was initially developed in [26] leading to the famous N-L means filter. It can be considered as a type of smart average filtering that uses the fact that similar pixels are not necessarily neighbors. Given two pixels, the similarity measure is the Euclidean distance between patches within their respective neighborhoods. Note that the Euclidean distance is more appropriate in white noise cases [26]. For the noise model (2), Coupé *et al.* [3] presented the OBNLM algorithm in which the Pearson distance was used along with an optimized version of the N-L means filter.

Variational methods. The variational approach is based on the minimization of a functional involving a data-fidelity term and a regularity assumption. A common assumption is that images belong to bounded variation spaces, and so total variation (TV) is often used for the regularization term [27]. For AWGN models, the fidelity term is simply given as the Euclidean distance between the unknown image and the corrupted image. Adaptations to model (2) consist in dividing the fidelity term by the unknown image to the power γ , which is also the standard deviation of the noise. The reader is referred to papers by Rudin, Lions and Osher [28] for the case $\gamma = 1$ and by Jin and Yang [4] for $\gamma = 0.5$. However, the functional cannot be minimized via simple primal dual algorithms [29] as in the AWGN case: a gradient descent is required.

Variance stabilization methods in the image processing literature focus mainly on Poisson or Poisson-Gaussian noise models arising in fluorescence microscopy. The Anscombe transform is often used for such a task (see, for example, Makitalo and Foi [30][31] and Boulanger *et al.* [32]). Zhang *et al.* [33] used a multiscale procedure that is also relying on a local normalization of wavelet coefficients. To the best of our knowledge, variance stabilization for the noise model (2) has never been considered beyond the one-dimensional case. In the following section we propose a technique to adapt the wavelet-based methods to this model. Moreover, we present a data-driven algorithm that solves the problem without prior knowledge of the parameters σ and γ of model (2).

III. METHOD

Hyperbolic wavelet bases are unconditional bases for functions in $L^2([0, 1]^2)$. They produce sparse representations so that the simple hard thresholding procedure provides estimators with very good theoretical and practical performances [7][8].

A. Notations

We begin with the hyperbolic wavelet transform (HWT). The starting point is a one-dimensional function ψ , called the mother wavelet, to which one can associate dilated and translated versions $\psi_{j,k}(\cdot) = 2^{j/2}\psi(2^j \cdot - k)$ with $j \geq 0$ and $k \geq 0$. In the same manner, a scaling function φ is defined, along with its dilated and translated versions $\varphi_{j,k}(\cdot) = 2^{j/2}\varphi(2^j \cdot - k)$. Then the 2D hyperbolic wavelet basis of $L^2([0, 1]^2)$ is given by

$$\begin{aligned} \psi_{j_1, j_2, k_1, k_2}(x_1, x_2) &= \psi_{j_1, k_1}(x_1)\psi_{j_2, k_2}(x_2), \\ \psi_{0, j_2, k_1, k_2}(x_1, x_2) &= \varphi_{0, k_1}(x_1)\psi_{j_2, k_2}(x_2), \\ \psi_{j_1, 0, k_1, k_2}(x_1, x_2) &= \psi_{j_1, k_1}(x_1)\varphi_{0, k_2}(x_2), \\ \psi_{0, 0, k_1, k_2}(x_1, x_2) &= \varphi_{0, k_1}(x_1)\varphi_{0, k_2}(x_2), \end{aligned} \quad (3)$$

for all $(j_1, j_2) \in \mathbb{N} \times \mathbb{N}$ and $(k_1, k_2) \in \mathbb{Z}^2$. This construction differs from that of the classical two-dimensional discrete wavelet transform (DWT), in the sense that different dilation factors are used in each dimension. In the case of the standard 2D DWT, only the cases $j_1 = j_2$ are allowed; therefore the resulting atoms are isotropic.

Let us note $I = \{\underline{j} = (j_1, j_2) \in \mathbb{N}^2 \text{ and } \underline{k} = (k_1, k_2) \in \mathbb{Z}^2\}$. The projection of a function f of $L^2([0, 1]^2)$ onto the HWT basis gives a set of hyperbolic wavelet coefficients $\{d_{\underline{j}, \underline{k}}\}_{(\underline{j}, \underline{k}) \in I}$ where:

$$d_{\underline{j}, \underline{k}}(f) = \langle \psi_{\underline{j}, \underline{k}}, f \rangle. \quad (4)$$

The set $\{d_{\underline{0}, \underline{k}}\}$, where $\underline{0} = (0, 0)$, represents the approximation coefficients. In finite discrete settings, a maximum scale is fixed at $J = \log_2(N)$ for an $N \times N$ image. Given that the HWT can be seen as a tensor product of one-dimensional wavelet transforms, its numerical implementation can be achieved by applying two successive 1D DWT to each of the two dimensions. Figure 1 highlights the difference of the scale-space tiling in the standard and hyperbolic settings.

B. Wavelet denoising

When the noisy observation v verifies model (1), the very simple, but powerful, procedure of wavelet thresholding mentioned earlier can be used. In the wavelet domain, the additive model (1) reads:

$$d_{\underline{j}, \underline{k}}(v) = d_{\underline{j}, \underline{k}}(u) + d_{\underline{j}, \underline{k}}(\varepsilon), \quad (5)$$

with $(\underline{j}, \underline{k}) \in I$. The hard thresholding estimator \hat{u}_σ is given by:

$$\hat{u}_\sigma = \sum_{(\underline{j}, \underline{k}) \in I_\sigma} d_{\underline{j}, \underline{k}}(v)\psi_{\underline{j}, \underline{k}}, \quad (6)$$

where $I_\sigma = \{(\underline{j}, \underline{k}) \in I, \text{ such that } |d_{\underline{j}, \underline{k}}(v)| > t(\sigma)\}$ and $t(\sigma)$ is the threshold parameter. Moreover, one of the distinctive features of this procedure is the existence of a *universal threshold* given by:

$$\begin{aligned} t(\sigma) &= \left\{ \log(\text{Card}(I))\text{Var}(d_{\underline{j}, \underline{k}}(\varepsilon)) \right\}^{1/2}, \\ &= \sigma \left\{ 2 \log(N^2) \right\}^{1/2}. \end{aligned} \quad (7)$$

In image restoration, we often model the unknown image as an element of an anisotropic function space, i.e., the regularity parameters are allowed to be different along the different dimensions. This notion of anisotropy is at the heart of multivariate function estimation [7]. Hyperbolic wavelets are well suited to such situations [34]. It has recently been shown [9] that mixing scales when constructing wavelets, as in (3), makes thresholding techniques comparable to state-of-the-art denoising algorithms. The choice of the threshold (7) is crucial and is based on the fact that the wavelet coefficients are Gaussian and independent. In the next section we show how, in the case of the ultrasound noise model (2), this obstacle can be overcome via a wavelet-based variance stabilization technique.

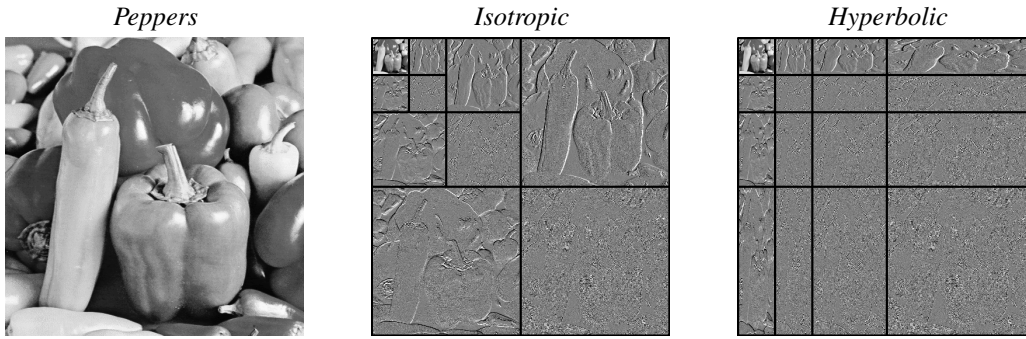


Figure 1: Wavelet decomposition in isotropic and hyperbolic settings.

C. The wavelet-Fisz approach

In (2), the noise component takes the form:

$$\eta = u^\gamma \varepsilon. \quad (8)$$

Therefore, its variance depends on the unknown image. To obtain an adaptive image-dependent threshold, we extend the results from [6] to our specific two-dimensional problem.

Lemma 3.1: Let $\{\psi_{\underline{j},\underline{k}}\}_{(\underline{j},\underline{k}) \in I}$ be a normalized wavelet basis, such that $\|\psi\|_2^2 = 1$. Let $u_{\underline{j},\underline{k}}$ denote the restriction of u to the support of the function $\psi_{\underline{j},\underline{k}}$. Assume that, we are given for each $(\underline{j},\underline{k}) \in I$, a constant function $\bar{u}_{\underline{j},\underline{k}}$ converging to $u_{\underline{j},\underline{k}}$ as $j_1, j_2 \rightarrow \infty$. Then we have:

$$\left\{ \frac{d_{\underline{j},\underline{k}}(\eta)}{\bar{u}_{\underline{j},\underline{k}}^\gamma} \right\}_{\underline{j},\underline{k}} \xrightarrow{d} \mathcal{N}(0, \sigma), \text{ as } j_1, j_2 \rightarrow \infty. \quad (9)$$

Since the noise is assumed to be a centered Gaussian random variable, the vector $\{d_{\underline{j},\underline{k}}(\eta)/\bar{u}_{\underline{j},\underline{k}}^\gamma\}_{\underline{j},\underline{k}}$ is normal with zero mean. In Appendix A, we derive the asymptotic variance when given in (9). Convergence results follow from the one-dimensional case [6]. The idea of applying this Gaussianizing routine to wavelets coefficients was first introduced for *Poisson* intensity estimation by Fryzlewicz and Nason [35], following a general framework introduced by Fisz [36]¹. It was later extended to *Poisson* intensity estimation in images [37]. An approximation $\bar{u}_{\underline{j},\underline{k}}$ of the unknown image u needs to be computed in the support of the function $\psi_{\underline{j},\underline{k}}$. A key point here is the use of the low-frequency outputs of the wavelet transform at each scale as local means pre-estimations. These outputs are given by scaling coefficients:

$$c_{\underline{j},\underline{k}}(f) = \langle \varphi_{\underline{j},\underline{k}}, f \rangle, \quad (10)$$

where

$$\varphi_{j_1, j_2, k_1, k_2}(x_1, x_2) = \varphi_{j_1, k_1}(x_1) \varphi_{j_2, k_2}(x_2). \quad (11)$$

The support of the function $\varphi_{\underline{j},\underline{k}}$ decreases as the value $|\underline{j}| = j_1 + j_2$ increases. As a consequence of the law of large numbers, the local means approximation (10) becomes less accurate. This has limited consequences since, following [6], we consider only the coarsest scales up to a certain level

$|\underline{j}| \leq J_{max}$. Not much information is lost since the finest scales consist of high-frequency components, which are essentially noise. Using lemma 3.1, we can now define a new set for the construction of the nonlinear estimator (6) given by:

$$\tilde{I}_\sigma = \{(\underline{j}, \underline{k}) \in I, \text{ s.t } |\underline{j}| \leq J_{max}; \frac{|d_{\underline{j},\underline{k}}(v)|}{\sigma c_{\underline{j},\underline{k}}(v)^\gamma} > t(1)\}. \quad (12)$$

Implementation: The wavelet-Fisz (WF) technique can be performed using the non-decimated wavelet transform (NDWT) introduced in [38]. The wavelet coefficients magnitudes (4) and the approximation coefficients (10) for the NDWT are presented in Figure 2. It has been shown that the denoising methods based on NDWT outperforms those based on traditional (decimated) wavelets in terms of the mean-squared error (MSE) and the signal-to-noise ratio (SNR) [39]. This is mainly due to its translation invariance. However, the non-decimated wavelet coefficients are, in general, correlated even if the noise is uncorrelated. The choice of relevant wavelet coefficients becomes a correlated multiple hypothesis-testing problem. Thus, the choice of the threshold (7) can lead to non-optimal results. In practice, one can consider the non-decimated wavelet coefficients as separate packets of uncorrelated coefficients [40]. The universal threshold can then be applied to each packet. The pseudo-code for the routine is given in Algorithm 1.

Algorithm 1 WF algorithm

Input: $f, \sigma, \gamma, J_{max}$

Output: Estimate \tilde{u}

- 1: $[d_{\underline{j},\underline{k}}, c_{\underline{j},\underline{k}}] \leftarrow \text{NDWT}(f)$
 - 2: **for** each couple $(\underline{j}, \underline{k})$ **do**
 - 3: **if** $|\underline{j}| > J_{max}$ **then** $d_{\underline{j},\underline{k}} = 0$
 - 4: **else**
 - 5: $p_{\underline{j},\underline{k}} = \sigma \times (c_{\underline{j},\underline{k}})^\gamma$
 - 6: $s_{\underline{j},\underline{k}} = |d_{\underline{j},\underline{k}}|/p_{\underline{j},\underline{k}}$
 - 7: **if** $s_{\underline{j},\underline{k}} < t(1)$ **then** $d_{\underline{j},\underline{k}} = 0$
 - 8: **end if**
 - 9: **end if**
 - 10: **end for**
 - 11: $\tilde{u} = \text{INDWT}(d_{\underline{j},\underline{k}})$
-

¹Hence the name wavelet-Fisz.

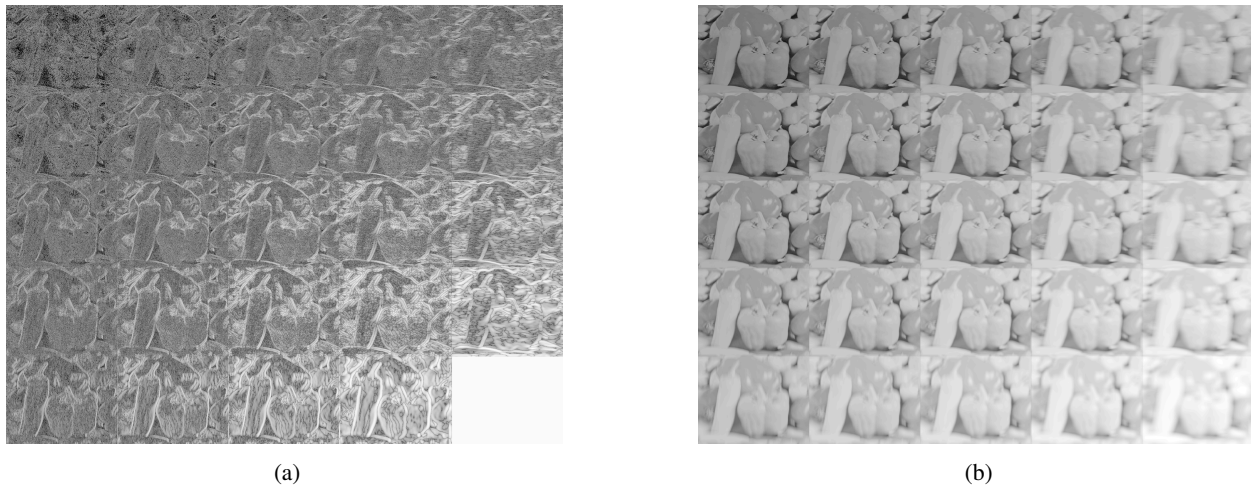


Figure 2: Outputs of the hyperbolic NDWT of the *Peppers* image: (a) the set of wavelet coefficients $\{d_{j,k}\}_{j,k}$ and (b) the set of approximation coefficients $\{c_{j,k}\}_{j,k}$.

The key step in this algorithm is the stabilization technique leading to the set $\{s_{j,k}\}_{(j,k) \in I}$. Figure 3 shows how the wavelet coefficients are stabilized after the WF procedure (with $\sigma = 2$ and $\gamma = 0.5$). We rescaled the wavelet coefficients magnitudes between 0 and 1 and fit a normal distribution. The *Liver* image represents a section of a human liver along with the portal vein. The diagonal details of the wavelet transform at the first thresholding scale are examined. At fine scales, the wavelet transformation mainly retrieves the noise component. We can clearly see that the distribution of the wavelet coefficients deviates from the Gaussian distribution. This phenomenon can be explained by model (2) given that the noise is perturbed by the image statistics. In fact, it was observed that the statistics of the wavelet coefficients of an image are more likely to follow distributions with heavier tails than a *Gaussian* distribution, such as *Exponential* and *Laplacian* distributions [41][42]. Note that the non-Gaussianity of the wavelet coefficients distribution in US images was first observed by Achim *et al.* [20]. In this work, the authors assumed that the noise had an alpha-stable distribution.

D. Fully data-driven extension

Beyond the fact that there is no conventional noise model in ultrasound imaging, different authors may use different parametrizations for a given noise model. In particular, for our model of interest, different values for the parameters σ and γ are given in [3],[4] and [28]. A point of debate is whether a large value should be used for γ and a small one for σ or vice-versa. We sidestep the problem by estimating the standard deviation of the noise directly from the data. Here, we follow the work of Fryzlewicz and Delouille [43] who developed extensions of the wavelet-Fisz algorithm that adapt to models with unknown variance. This was applied, for instance, to the variance stabilization and normalization of one-color microarray data [44]².

²An R software package (DDHFm) for this routine is available on the web: <https://cran.r-project.org/web/packages/DDHFm/index.html>

1) *Standard deviation estimation*: To address this problem, any filter with low computational cost can be used on the noisy image to obtain a pre-estimation \bar{u} . We applied a simple mean filter of size M to our images. An estimation of the noise component η is then given by the residual:

$$\hat{\eta}(\bar{u}) = v - \bar{u} \quad (13)$$

To estimate the variance, a kernel-smoothing technique is applied to the highly oscillating squared residuals $\hat{\eta}^2$. For any vector w with values belonging to $[\min(\bar{u}), \max(\bar{u})]$, the variance estimator of w is given as:

$$h(w) = \widehat{\text{Var}}(\hat{\eta}(w)) = \frac{\langle \hat{W}_b(w), \hat{\eta}^2 \rangle}{\hat{W}_b(w)}, \quad (14)$$

where W is defined as:

$$\hat{W}_b(w) = \frac{1}{N^2 b} K\left(\frac{\bar{u} - w}{b}\right), \quad (15)$$

with b the bandwidth of the kernel K . This regression technique is called the Nadaraya-Watson estimation. Under the assumption that the variance of the noise is a positive power of the image intensity, as suggested by model (2), it is natural to constrain the estimator of the variance to be non-decreasing. This can be done using the so-called isotonic regression [45], which consists in finding the closest non-decreasing function, in terms of the least mean square error, using a “pool-adjacent-violators” algorithm [46]. We present an example of this type of routine on a corrupted 512×512 *Peppers* image. Our choice of the *Peppers* image is motivated by the fact that it has many variations in grey values, resulting in an interval of intensities well covered by the vector w . The global regularity of the image is the main criterion for the choice of the size M of the average filter. In fact, a compromise is required; M should be chosen as large as possible with respect to the homogeneity of the image. Small values are required for M if the image has many discontinuities. We investigated various choices for the size M of the average filter. We found that a

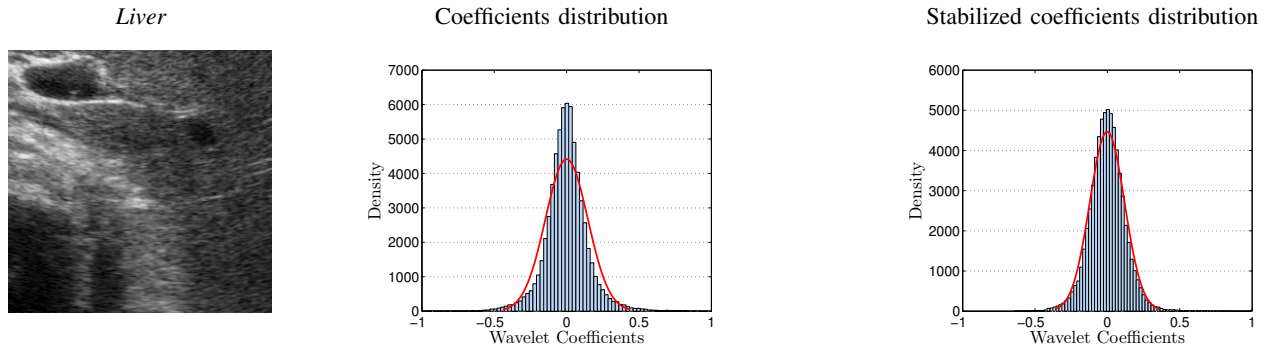


Figure 3: Wavelet decomposition of US images: Statistics of the diagonal details at the finest scale.

value of $M = 12$ gives a reliable pre-estimation of the image. In general we recommend the use of this value for images with a moderate number of discontinuities such as the *Peppers* image. Naturally, M also depends on the resolution of the image; this dependence is expected to be linear. The bandwidth b has less influence on the estimator than M because of the regression step, which corrects remaining oscillations. This was also pointed out by Fryzlewicz [6]. A value of $b = 3$ was found to be stable. In the paper we fix this value and tune only M . The results of two experiments with different values of γ and σ are given in Figure 4. As the image pixel values range from 0 to 255, we simply choose w to be a uniform discretization of $[0, 255]$. The results confirm the reliability of the standard deviation estimator $h^{1/2}$ in comparison to the ground truth.

required in the inputs. Equation (17) suggests replacing step 5 in Algorithm 1 with:

$$p_{j,\underline{k}} = h^{1/2}(c_{j,\underline{k}}), \quad (18)$$

IV. EXPERIMENTS AND DISCUSSION

In this section, some experiments evaluating the performance of the WF method are presented. To distinguish the different contributions of this work, we divide this section into two parts. First, the performance of the WF method for both isotropic (IWF) and hyperbolic (HWF) constructions are compared, and then the potentials of the data-driven extension are shown.

A. The WF method

Herein, the results of the WF method are compared to those obtained using two other approaches that consider the noise model given by equation (2). The OBNLM filter has proven to be very effective in speckle noise reduction [3]. On the other hand, the variational approach [4] is an adaptation of the well-established TV denoising to model (2). The criteria used for the comparisons were the classical peak signal-to-noise-ratio (PSNR) and the structural similarity index measure (SSIM) [47], which assessed the tissue structure preservation. Since ultrasound imaging is not usually used for functional studies, the preservation of morphological information while performing denoising is more important than preserving the true measured pixel intensity. We also show the difference between the true image and the denoised result of every method. This is known in the literature as the method noise [26]. One expects to retrieve more noise in areas of high pixel intensities according to model (2). The OBNLM filter is available on the web³. The parameters α and M controlling the number of blocks and the size of the search window were fixed at 3 and 6, as in the original paper, and the filtering parameter h was optimized for different levels of noise. The variational algorithm was implemented with the gradient descent step fixed at 0.2, as suggested by the authors. We used *Haar* wavelets for the WF method. The scaling function associated with these wavelets behaves like a simple mean filter, which results in a reliable set of approximation coefficients $\{c_{j,\underline{k}}\}_{j,\underline{k}}$. These

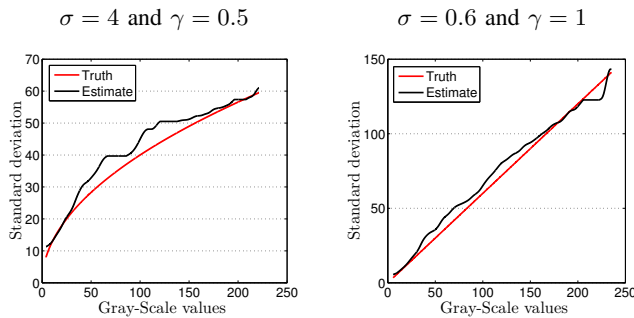


Figure 4: Standard deviation estimation from experiments on the *Peppers* image for different values of σ and γ .

2) *Blind denoising*: We describe the adaptation of the WF algorithm to the fully data-driven methodology. For our noise model, the standard deviation estimator presented in III-D1 gives the following approximation:

$$h^{1/2}(w) \approx \sigma w^\gamma. \quad (16)$$

Hence, we have a similar result to that given in lemma 3.1

$$\left\{ \frac{d_{j,\underline{k}}(\eta)}{h^{1/2}(c_{j,\underline{k}})} \right\}_{j,\underline{k}} \xrightarrow{d} \mathcal{N}(0, 1), \quad (17)$$

when $j_1, j_2 \rightarrow \infty$. In Algorithm 1, the parameters σ and γ appear in auxiliary step 5 for the computation of the variance in the wavelet supports. To obtain a data-driven version of this algorithm, the knowledge of σ and γ should not be

³<https://sites.google.com/site/pierrickcoupe>

wavelets are also efficient at preserving discontinuities. We are aware, however, that these wavelets do not provide optimal results in terms of PSNR and it is possible to improve the results using wavelets from other families such as Daubechies or Coiflets. In all experiments, the coefficients corresponding to the first finest scale are truncated.

1) *Experiments on synthetic data:* Two experiments were conducted by adding synthetic noise to clean images. We set $\gamma = 0.5$, as in [3] and [4]. The *Blocks* image aims only at demonstrating the ability of hyperbolic wavelets to deal with highly anisotropic images. In fact, this image is an additive model where the regularities in the two space dimensions are distinct. This is a highly anisotropic case, which favors the hyperbolic construction [8]. The *Kidney* image is a CT image taken from the FIELD II website⁴. This example is challenging to denoise because of the presence of many gray level variations.

Table I reports the performance of the different methods with their optimal parameters. In the case of the *Blocks* image, the contribution of the hyperbolic setting is clearly visible in terms of PSNR, SSIM and visual quality (e.g., Figure 5). The hyperbolic wavelet-Fisz thresholding gave the best results for all noise levels. The variational approach also gave good results because the image is piece-wise constant. Yet, it suffers from blurring effects around the edges. Artifacts caused by the patching process are clearly visible in the OBNLM filter results. In the case of the *Kidney* image, our approach did not outperform the OBNLM filter and the variational method in terms of PSNR, but remains competitive. This can be explained by the different philosophy of wavelet thresholding methods, which are more oriented toward the complete elimination of noise rather than the minimizing the MSE [5]. The OBNLM approach performed well when in the presence of low noise levels. Conversely, the variational method performed better for high noise levels. As can be observed in Figure 6, the wavelet approaches efficiently preserved the structure. Unfortunately, we note the presence of artifacts associated with the supports of the wavelet basis. This is a common disadvantage of wavelet thresholding methods. The method noise presented in Figure 7 shows the structure of the removed noise for each method. It can be observed that, for all methods, the removed noise component has higher values in high-intensity areas in coherence with the noise model (2). Moreover, the proposed method produce a good compromise between efficient noise removal and preservation of structures, in the sense that the different regions are easily distinguishable. Another advantage of wavelet thresholding is its adaptability; the threshold comes directly from the knowledge of σ and γ . Tuning the OBNLM filter is less straightforward, as the algorithm parameters are not explicitly expressed in terms of the model parameters.

2) *Experiments on real data:* We evaluated our algorithm on samples from real US imaging. The blind extension of the SSIM presented in [48] was not suitable here because the noise is signal-dependent. Therefore, comparisons and parameter tuning were entirely based on the visual quality of the resulting

image. We applied the different set of parameters in Table I and chose those giving the best results. The first test concerns the *Carotid-Thyroid* image. The speckle stemming from blood flow can be seen on the left, while the thyroid gland is visible on the right. Denoising such images may be a pre-processing step in segmentation of the thyroid gland. An enhanced image also eases the tracking of the carotid artery wall in dynamic imaging. The second test examines Cranial US images. This technique is mostly used for babies, before the cranial bones have closed, as the US waves cannot pass through the skull. For instance, it is used to obtain information on complications related to premature birth.

The results of the different algorithms applied to the *Carotid-Thyroid* image are shown in Figure 8. The image obtained using the variational method is clearly blurred; this is due to the piecewise constancy constraint of total variation. The OBNLM filter achieved a better result, although there was some visible partitioning in the final image. The proposed method gave an image with well-defined structures because of the local treatment of the wavelet paradigm. Moreover, in the hyperbolic case, one can see that the horizontal structures are satisfactorily recovered. The main artifact with the proposed method is the occurrence of wavelet basis atoms in the final image. Figure 9 illustrates how these artifacts can be drastically reduced when the hyperbolic wavelet is used. In the image obtained using the IWF procedure, small regions representing the supports of the *Haar* basis can be seen. These are similar to the artifacts related to patching that occurred using the non-local methods. An improved result is obtained using the hyperbolic settings, even though some lines are still visible.

B. The data-driven WF method

In this section, the experiments reveal the potential of the data-driven extension of our algorithm. Table II presents a comparison of the results obtained using HWF and data-driven HWF (dHWF) for the *Peppers* image studied in Figure 4. As expected, there is a loss, proportional to the noise level, in the PSNR and the SSIM up to 0.5 dB and 4%, respectively. We believe this loss is acceptable, especially when the noise level is not very high. We applied this data-driven technique to the 256×256 *Liver* image studied in Figure 3. This image has a few discontinuities, allowing the use of a large window for the mean filter. Here, we used a window of size $M = 8$. The experiments were conducted using a PC DELL Latitude E6430 with an Intel Core i7-3740QM CPU, 2.7 GHZ processor and 8 GB of RAM under Fedora 20, using MATLAB v.8.2.0.701, 64-bit. The recorded run-time for HWT was 40.72 s while it was 54.51 s for dHWT. The difference in timings is due to the different routines of the variance estimation step. The results are given in Figure 10. The first interesting result is the “non-constant slope” of the estimated standard deviation. This demonstrates that model (1) cannot be used. We suspect that this function is proportional to the power of the image, thereby giving image processing-based evidence of the relevance of the noise model (2) directly from the data. It was also noted that the set of wavelet coefficients was properly stabilized. We

⁴<http://field-ii.dk>

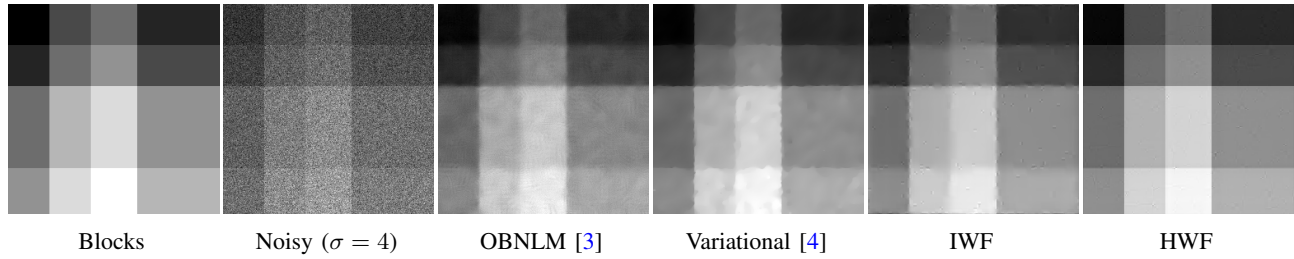


Figure 5: Results of various methods applied to the *Blocks* image. The quantitative evaluation is given in Table I.

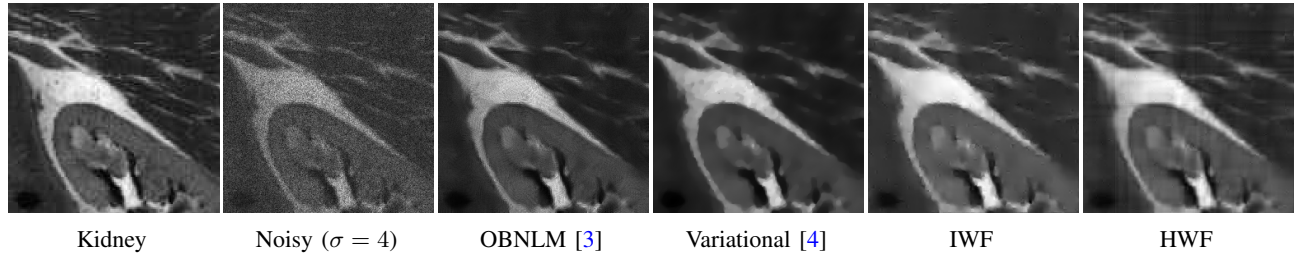


Figure 6: Results of various methods applied to the *Kidney* image. The quantitative evaluation is given in Table I.

	Blocks			Kidney		
	PSNR (dB)	SSIM	Parameters	PSNR (dB)	SSIM	Parameters
Noisy($\sigma = 2$)	22.83	0.135	–	24.83	0.430	–
OBNLM [3]	35.13	0.917	$h=1.5$	30.05	0.845	$h=1$
Variational [4]	37.98	0.972	$n_{iter}=180$	28.72	0.814	$n_{iter}=160$
IWF	35.78	0.958	–	29.04	0.837	–
HWF	49.65	0.993	–	30.24	0.866	–
Noisy($\sigma = 3$)	20.95	0.071	–	22.30	0.272	–
OBNLM [3]	32.86	0.836	$h=2$	28.71	0.752	$h=1$
Variational [4]	35.57	0.955	$n_{iter}=260$	27.91	0.799	$n_{iter}=180$
IWF	33.75	0.929	–	27.39	0.791	–
HWF	46.65	0.987	–	28.20	0.822	–
Noisy($\sigma = 4$)	19.31	0.044	–	20.83	0.187	–
OBNLM [3]	31.38	0.739	$h=2.5$	27.81	0.765	$h=2$
Variational [4]	34.41	0.946	$n_{iter}=350$	28.03	0.782	$n_{iter}=210$
IWF	32.40	0.909	–	26.63	0.764	–
HWF	43.04	0.973	–	27.31	0.791	–

Table I: Quantitative comparison (PSNR & SSIM) and optimal parameters for different methods applied to the *Blocks* and *Kidney* images with different noise levels.

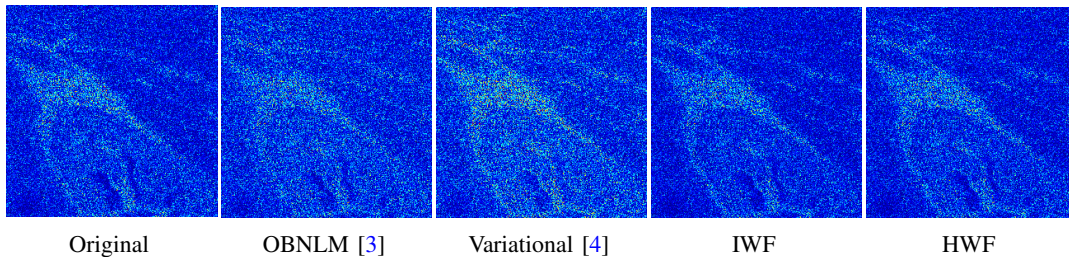


Figure 7: The method noise [26] of the various approaches applied to the *Kidney* image ($\sigma = 3$).

compared the image obtained in the data-driven mode to the one obtained using an exhaustive search for the parameter σ with $\gamma = \{0.5; 1\}$. The results demonstrated that the data-driven result is satisfying and less blurred.

V. CONCLUSION

In this paper, we described a novel approach for denoising ultrasound images based on wavelet thresholding, variance stabilization and the use of the hyperbolic wavelet basis. The quantitative and visual results show the potential of the proposed method and the utility of the hyperbolic construction.

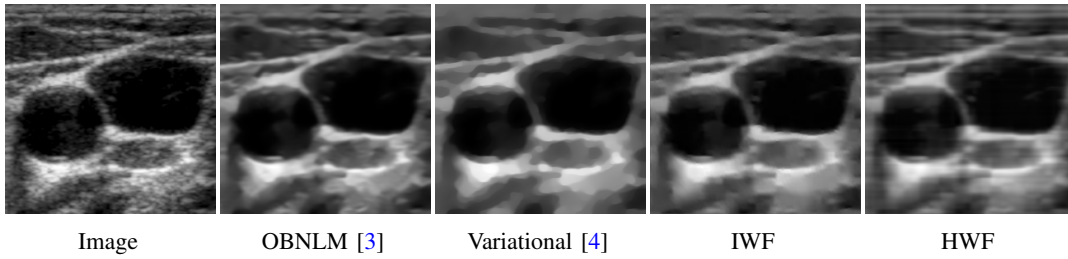


Figure 8: Visual evaluation of various methods applied to the *Carotid-Thyroid* image.

σ	PSNR (dB)			SSIM		
	2	3	4	2	3	4
Noisy	20.21	16.65	14.16	0.35	0.23	0.16
HWF	29.25	27.65	26.44	0.78	0.75	0.73
dHWF	29.09	27.40	26.17	0.76	0.72	0.69

Table II: Denoising of the *Peppers* image: Quantitative comparison (PSNR & SSIM) of the HWF and its fully data-driven version for different noise levels.

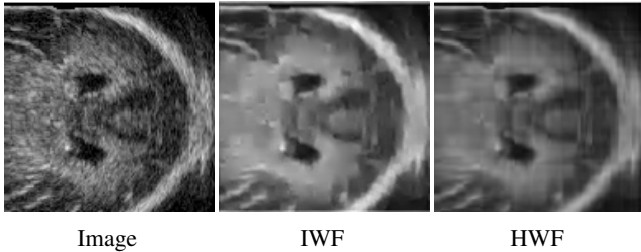


Figure 9: Visual comparison between IWF and HWF for the *brain* image.

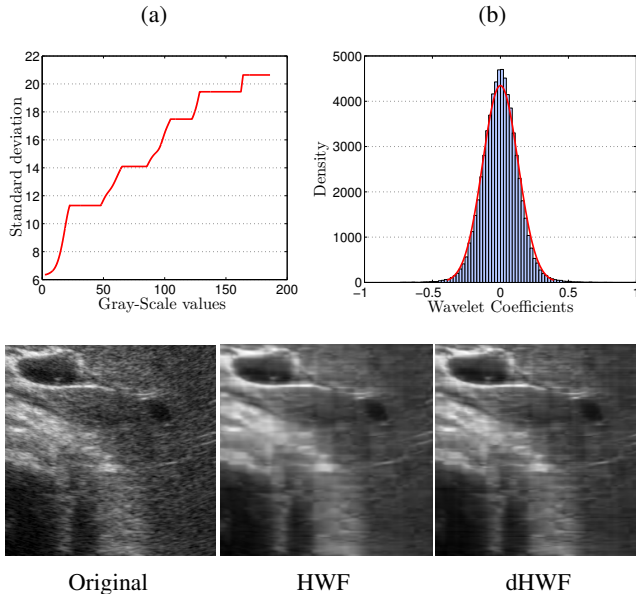


Figure 10: Experiments on the *Liver* image: (a) estimated standard deviation, (b) blind stabilized Coefficients.

A data-driven extension of the method is also presented. When applied to real data, this extension provides evidence that the noise model is relevant. We also believe that a method

free of tuning requirements is highly desirable, especially for physicians. The extension to three-dimensional wavelets can be used for two purposes: 3D denoising or (2D+t) dynamic US denoising. While the 3D case is straightforward, the dynamic US case must be handled carefully because the noise variance depends only on the spatial dimension. Thus, the variance stabilization and the local means approximation should be performed only on the spatial variables. We are currently addressing this issue.

APPENDIX A VARIANCE DERIVATION

We recall that $\eta = u^\gamma \varepsilon$, and we note $t = (t_1, t_2)$

$$\begin{aligned} \text{Var} \left\{ \frac{d_{j,k}(\eta)}{\bar{u}_{j,k}^\gamma} \right\} &= \frac{1}{\bar{u}_{j,k}^{2\gamma}} \text{Var} \left\{ \sum_t \psi_{j,k}(t) u^\gamma(t) \varepsilon(t) \right\}, \\ &= \frac{\sigma^2}{\bar{u}_{j,k}^{2\gamma}} \sum_t \psi_{j,k}^2(t) u^{2\gamma}(t), \\ &= \frac{\sigma^2}{\bar{u}_{j,k}^{2\gamma}} \sum_t \psi_{j,k}^2(t) u_{j,k}^{2\gamma}(t). \\ &= \sigma^2 \sum_t \frac{u_{j,k}^{2\gamma}(t)}{\bar{u}_{j,k}^{2\gamma}} \psi_{j,k}^2(t). \end{aligned}$$

Finally, since when $j_1, j_2 \rightarrow \infty$, $\bar{u}_{j,k}$ converges to $u_{j,k}$, then for each t in the support of $\psi_{j,k}$, we have:

$$\lim_{\bar{u}_{j,k} \rightarrow u_{j,k}} \frac{u_{j,k}^{2\gamma}(t)}{\bar{u}_{j,k}^{2\gamma}} = 1.$$

Thus:

$$\text{Var} \left\{ \frac{d_{j,k}(\eta)}{\bar{u}_{j,k}^\gamma} \right\} = \sigma^2 \sum_t \psi_{j,k}^2(t) = \sigma^2 \|\psi_{j,k}\|_2^2 = \sigma^2.$$

REFERENCES

- [1] D. Kaplan and Q. Ma, "On the statistical characteristics of the log-compressed Rayleigh signals: theoretical formulation and experimental results," *J. Acoust. Soc. Am.*, vol. 95, pp. 1396–1400, 1994.
- [2] T. Loupas, W. McDicken, and P. Allan, "An adaptive weighted median filter for speckle suppression in medical ultrasonic images," *IEEE Trans. Circuits and Systems*, vol. 36, pp. 129–135, 1989.
- [3] P. Coupé, P. Hellier, C. Kervrann, and C. Barillot, "Nonlocal means-based speckle filtering for ultrasound images," *IEEE Trans. Image Process.*, vol. 18, no. 7, pp. 2221–2229, 2009.

- [4] Z. Jin and X. Yang, "A variational model to remove the multiplicative noise in ultrasound images," *Journal of Mathematical Imaging and Vision*, vol. 39, no. 1, pp. 62–74, 2011.
- [5] D. L. Donoho and I. M. Johnstone, "Ideal spatial adaptation by wavelet shrinkage," *Biometrika*, vol. 81, pp. 425–455, 1994.
- [6] P. Fryzlewicz, "Data-driven wavelet-Fisz methodology for nonparametric function estimation," *Electronic Journal of Statistics*, vol. 2, pp. 863–896, 2008.
- [7] M. H. Neumann, "Multivariate wavelet thresholding in anisotropic function spaces," *Statistica Sinica*, vol. 10, pp. 399–431, 2000.
- [8] F. Autin, G. Claeskens, and J. Freyermuth, "Asymptotic performance of projection estimators in standard and hyperbolic wavelet bases," *Electronic Journal of Statistics*, vol. 9, no. 2, pp. 1852–1883, 2015.
- [9] N. Remenyi, O. Nicolis, G. Nason, and B. Vidakovic, "Image denoising with 2-D scale-mixing complex wavelet transforms," *IEEE Trans. Image Process.*, vol. 23, no. 12, pp. 5165–5174, 2014.
- [10] Y. Yu and S. T. Acton, "Speckle reducing anisotropic diffusion," *IEEE Trans. Image Process.*, vol. 11, no. 11, pp. 1260–1270, 2002.
- [11] K. Krissian, C. F. Westin, R. Kikinis, and K. G. Vosburgh, "Oriented speckle reducing anisotropic diffusion," *IEEE Trans. Image Process.*, vol. 16, pp. 1412–1424, 2007.
- [12] G. Ramos-Llorden, G. Vegas-Sanchez-Ferrero, M. Martin-Fernandez, and C. Alberola-Lopez, *IEEE Trans. Image Process.*, vol. 24, no. 1, pp. 345–358.
- [13] J. W. Goodman, "Statistical properties of laser speckle patterns," in *Laser Speckle and Related Phenomena*. Springer, 1975, pp. 9–75.
- [14] R. F. Wagner, S. W. Smith, J. M. Sandrik, and H. Lopez, "Statistics of speckle in ultrasound b-scans," *IEEE Trans. Sonics and Ultrasonics*, vol. 30, no. 3, pp. 156–163, 1983.
- [15] J.-S. Lee, "Digital image enhancement and noise filtering by use of local statistics," *IEEE Trans. Pattern Anal. Mach. Intell.*, vol. 2, no. 2, pp. 165–168, 1980.
- [16] V. S. Frost, J. A. Stiles, K. S. Shanmugan, and J. C. Holtzman, "A model for radar images and its application to adaptive digital filtering of multiplicative noise," *IEEE Trans. Pattern Anal. Mach. Intell.*, vol. 4, no. 2, pp. 157–166, 1982.
- [17] D. T. Kuan, A. A. Sawchuk, T. C. Strand, and P. Chavel, "Adaptive noise smoothing filter for images with signal-dependent noise," *IEEE Trans. Pattern Anal. Mach. Intell.*, vol. 7, no. 2, pp. 165–177, 1985.
- [18] P. Perona and J. Malik, "Scale-space and edge detection using anisotropic diffusion," *IEEE Trans. Pattern Anal. Mach. Intell.*, vol. 12, no. 7, pp. 629–639, 1990.
- [19] X. Zong, A. F. Laine, and E. A. Geiser, "Speckle reduction and contrast enhancement of echocardiograms via multiscale nonlinear processing," *IEEE Trans. Med. Imag.*
- [20] A. Achim, A. Bezerianos, and P. Tsakalides, "Novel Bayesian multiscale method for speckle removal in medical ultrasound images," *IEEE Trans. Med. Imaging*, vol. 20, no. 8, pp. 772–783, 2001.
- [21] G. Samorodnitsky and M. S. Taqqu, *Stable non-Gaussian random processes: Stochastic models with infinite variance*, ser. Stochastic modeling. New York: Chapman & Hall, 1994.
- [22] M. Sühling, M. Arigovindan, C. Jansen, P. Hunziker, and M. Unser, "Myocardial motion analysis from b-mode echocardiograms," *IEEE Trans. Image Process.*, vol. 14, no. 4, pp. 525–536, 2005.
- [23] T. Tuthill, R. Sperry, and K. Parker, "Deviation from Rayleigh statistics in ultrasonic speckle," *Ultrason. Imag.*, pp. 81–90, 1988.
- [24] G. Slabaugh, G. Unal, T. Fang, and M. Wels, "Ultrasound-specific segmentation via decorrelation and statistical region-based active contours," in *2006 IEEE Computer Society Conference on Computer Vision and Pattern Recognition (CVPR'06)*, vol. 1. IEEE, 2006, pp. 45–53.
- [25] D. Tenbrinck, S. Schmid, X. Jiang, K. P. Schäfers, and J. Stypmann, "Histogram-based optical flow for motion estimation in ultrasound imaging," *Journal of Mathematical Imaging and Vision*, vol. 47, no. 1-2, pp. 138–150, 2013.
- [26] A. Buades, B. Coll, and J.-M. Morel, "A non-local algorithm for image denoising," in *Proceedings of the 2005 IEEE Computer Society Conference on Computer Vision and Pattern Recognition (CVPR'05)*, vol. 2, 2005, pp. 60–65.
- [27] L. Rudin, S. Osher, and E. Fatemi, "Nonlinear total variation based noise removal algorithms," *Physica D*, vol. 60, pp. 259–268, 1992.
- [28] L. Rudin, P. L. Lions, and S. Osher, *Multiplicative denoising and deblurring: theory and algorithms*, ser. Geometric Level Set Methods in Imaging, Vision, and Graphics. S. Osher and N. Paragios, Eds., 2003.
- [29] L. Condat, "A generic proximal algorithm for convex optimization: application to total variation minimization," *Signal Process. Lett., IEEE*, vol. 21, no. 8, pp. 985–989, 2014.
- [30] M. Makitalo and A. Foi, "A closed-form approximation of the exact unbiased inverse of the aniscombe variance-stabilizing transformation," *IEEE Trans. Image Process.*, vol. 20, no. 9, pp. 2697–2698, 2011.
- [31] M. Mäkitalo and A. Foi, "Noise parameter mismatch in variance stabilization, with an application to Poisson-Gaussian noise estimation," *IEEE Trans. Image Process.*, vol. 23, no. 12, pp. 5348–5359, 2014.
- [32] J. Boulanger, C. Kervrann, P. Bouthemy, P. Elbau, J.-B. Sibarita, and J. Salamero, "Patch-based nonlocal functional for denoising fluorescence microscopy image sequences," *IEEE Trans. Med. Imag.*, vol. 29, no. 2, pp. 442–454, 2010.
- [33] B. Zhang, M. Fadili, J.-L. Starck, and J.-C. Olivo-Marin, "Multiscale variance-stabilizing transform for mixed-Poisson-Gaussian processes and its applications in bioimaging," in *2007 IEEE International Conference on Image Processing*, vol. 6. IEEE, 2007, pp. 233–236.
- [34] S. G. Roux, M. Clausel, B. Vedel, S. Jaffard, and P. Abry, "Self-similar anisotropic texture analysis: The hyperbolic wavelet transform contribution," *IEEE Trans. Image Process.*, vol. 22, no. 11, pp. 4353–4363, 2013.
- [35] P. Fryzlewicz and G. Nason, "A Haar-Fisz algorithm for Poisson intensity estimation," *Journal of Computational and Graphical Statistics*, vol. 13 (3), pp. 621–638, 2004.
- [36] M. Fisz, "The limiting distribution of a function of two independent random variables and its statistical application," *Colloquium Mathematicum*, vol. 3, pp. 138–146, 1955.
- [37] J. M. Fadili, J. Mathieu, B. Romaniuk, and M. Desvignes, "Bayesian wavelet-based Poisson intensity estimation of images using the Fisz transformation," in *Proc. International Conference on Image and Signal Processing, Agadir, Morocco*, 2003, pp. 242–253.
- [38] R. R. Coifman and D. L. Donoho, "Translation-invariant denoising," in *Antoniadis & Oppenheim, Wavelets and Statistics. Lecture Notes in Statistics*, pp. 125–150, 1995.
- [39] G. P. Nason and B. W. Silverman, "The stationary wavelet transform and some statistical applications," in *Antoniadis & Oppenheim, Wavelets and Statistics. Lecture Notes in Statistics*, pp. 281–300, 1995.
- [40] G. Nason, *Wavelet Methods in Statistics with R*. Springer Science & Business Media, 2010.
- [41] S. Mallat, *A Wavelet Tour of Signal Processing*. Academic Press, 1999.
- [42] S. Jaffard, "Beyond Besov spaces part 1: Distributions of wavelet coefficients," *Journal of Fourier Analysis and Applications*, vol. 10, no. 3, pp. 221–246, 2004.
- [43] P. Fryzlewicz and V. Delouille, "A data-driven Haar-Fisz transform for multiscale variance stabilization," in *IEEE/SP 13th Workshop on Statistical Signal Processing, 2005*. IEEE, 2005, pp. 539–544.
- [44] E. Motakis, G. P. Nason, P. Fryzlewicz, and G. Rutter, "Variance stabilization and normalization for one-color microarray data using a data-driven multiscale approach," *Bioinformatics*, vol. 22, no. 20, pp. 2547–2553, 2006.
- [45] P. Fryzlewicz, V. Delouille, and G. P. Nason, "GOES-8 X-ray sensor variance stabilization using the multiscale data-driven Haar-Fisz transform," *Journal of the Royal Statistical Society: Series C (Applied Statistics)*, vol. 56, no. 1, pp. 99–116, 2007.
- [46] P. Mair, K. Hornik, and J. de Leeuw, "Isotone optimization in r: pool-adjacent-violators algorithm (pava) and active set methods," *Journal of Statistical Software*, vol. 32, no. 5, pp. 1–24, 2009.
- [47] Z. Wang, A. C. Bovik, H. R. Sheikh, and E. P. Simoncelli, "Image quality assessment: From error visibility to structural similarity," *IEEE Trans. Image Process.*, vol. 13, no. 4, pp. 600–612, 2004.
- [48] X. Kong, K. Li, Q. Yang, L. Wenyan, and M.-H. Yang, "A new image quality metric for image auto-denoising," in *2013 IEEE International Conference on Computer Vision (ICCV)*. IEEE, 2013, pp. 2888–2895.

Younes Farouj received the M.Sc. degree in applied mathematics from the University of Toulouse in 2013. He is currently working towards the Ph.D. degree at the CREATIS Lab, affiliated to INSA de Lyon. His research interests include wavelets, anisotropic analysis and regularization, optimization, nonparametric/adaptive/data-driven estimation and their applications in biomedical signal and image processing.



Jean-Marc Freyermuth was born in Châlons-en-Champagne, France. He received the Ph.D degree in statistics from the Université Catholique de Louvain, Belgium, in 2011. He was an associate researcher at the ORSTAT group at the University of Leuven, Belgium (2011-2014) and later at the Statistical Laboratory at the University of Cambridge, U.K (2015-2016). He is currently a statistical consultant and lecturer in statistics at the University of Neuchâtel, Switzerland. His main research interests include wavelet methods in statistics and time series

analysis with applications to brain science.



Laurent Navarro received the Master degree in 2004 and the PhD degree in 2007. He is now Assistant Professor with Mines Saint-Etienne (Institut Mines-Télécom), member of the SAINBIOSE Lab and associated member of the LIMOS Lab. His research interests include signal, image and data processing in healthcare engineering, but also biomechanical simulation using Lattice Boltzmann method and Finite element method.



Marianne Clausel was born in Marseille, France, in 1974. She received the Ph.D. degree in applied mathematics from Paris-Est Créteil University, Paris, France, in 2008. Since September 2011, she has been an Associate Professor with the Laboratoire Jean Kuntzmann, Grenoble Alpes University, Grenoble, France. She received a five years grant from chaire CNRS-UJF from 2011 to 2016. Her current research interests include wavelet-based signal processing, machine learning with application to large scale data analysis and non parametric statistics.



Philippe Delachartre received the Ph.D. degree from INSA Lyon, France, in 1994. He is currently a Professor with INSA Lyon. His research interests include motion estimation, segmentation, denoising, medical image analysis, ultrasound signal processing and ultrasound imaging.